CCFE-PR(15)84

L. Li, Y. Q. Liu, Y. Liang, N. Wang, F. C. Zhong and Y. Liu

Screening of external magnetic perturbation fields due to sheared plasma flow

Screening of external magnetic perturbation fields due to sheared plasma flow

L. Li1,[2,3,] Y. Q. Liu[4,5,6], Y. Liang[2,1], N. Wang[2,7], F. C. Zhong[1,3] and Y. Liu[8]

[1]College of Science, Donghua University, Shanghai 201620, China
[2]Forschungszentrum Jülich GmbH, Institut für Energie- und Klimaforschung - Plasmaphysik, Jülich, Germany
[3]Member of Magnetic Confinement Fusion Research Centre, Ministry of Education, China
[4]CCFE, Culham Science Centre, Abingdon, OX14 3DB, UK
[5]Southwestern Institute of Physics, PO Box 432, Chengdu 610041, China
[6]Department of Earth and Space Science, Chalmers University of Technology, SE-412 96 Gothenburg, Sweden
[7]State Key Laboratory of Advanced Electromagnetic Engineering and Technology, Huazhong University of Science and Technology, Wuhan, Hubei 430074, China
[8]Dalian University of Technology, Dalian, China

Screening of external magnetic perturbation fields due to sheared plasma flow

L. Li[1,2,3*], Y. Q. Liu[4,5,6], Y. Liang[2,1], N. Wang[2,7], F. C. Zhong[1,3] and Y. Liu[8]

[1]College of Science, Donghua University, Shanghai 201620, China

[2]Forschungszentrum Jülich GmbH, Institut für Energie- und Klimaforschung - Plasmaphysik, Jülich, Germany

[3]Member of Magnetic Confinement Fusion Research Centre, Ministry of Education, China

[4]CCFE, Culham Science Centre, Abingdon, OX14 3DB, UK

[5]Southwestern Institute of Physics, PO Box 432, Chengdu 610041, China

[6]Department of Earth and Space Science, Chalmers University of Technology, SE-412 96 Gothenburg, Sweden

[7]State Key Laboratory of Advanced Electromagnetic Engineering and Technology, Huazhong University of Science and Technology, Wuhan, Hubei 430074, China

[8]Dalian University of Technology, Dalian, China

[*]E-Mail: l.li@fz-juelich.de

Abstract

Within the single fluid resistive magneto-hydrodynamic (MHD) model, systematic toroidal modelling efforts are devoted to investigate the plasma response induced screening of the applied external 3D magnetic field perturbations, in the presence of sheared toroidal flow. One particular issue of interest is addressed, when the local flow speed approaches zero at the perturbation rational surface inside the plasma. Subtle screening physics, associated with the favourable averaged toroidal curvature effect (the GGJ effect [Glasser A H et al 1975 Phys. Fluids **7** 875]), is found to play an essential role at slow flow near the rational surface, by *enhancing* the screening at reduced flow. A strong cancellation effect between different terms of the Ohm's law is discovered, leading to different screening physics in the GGJ regime, as compared to that of the conventional screening of the typical resistive-inertial regime occurring at faster flow. These modelling results may be applicable to interpret certain mode locking experiments, as well as type-I edge localized mode suppression experiments, with resonant magnetic field perturbations being applied to tokamak plasmas at low input toroidal torque.

1. Introduction

The plasma response to external magnetic field plays important role in understanding various three-dimensional (3D) physics relevant to tokamak plasmas, such as the resonant field amplification (RFA) [1-5], the active control of the resistive wall mode (RWM) with magnetic feedback [6-11], the mode locking [12, 13] and the error field correction [14-16], as well as the suppression or mitigation of the edge localized modes (ELMs) in H-mode plasmas using resonant magnetic perturbations (RMP)[17-20].

One key element of the plasma response to 3D fields is the screening of the magnetic pitch aligned resonant components. Perfect screening occurs if the plasma is assumed to be ideal (i.e. with vanishing resistivity), which is often the case in modelling the RFA and the RWM control experiments for high beta (high temperature) plasmas, where the plasma pressure often exceeds the no-wall Troyon beta limit for the ideal kink instability [21]. On the other hand, only partial screening occurs in a resistive plasma, which is often the adopted model for simulating tokamak experiments at lower beta. This is particularly relevant for the mode locking experiments due to field errors, as well as the ELM control experiments using RMP fields. Understanding the field screening phenomena in these low beta (below the Troyon limit), resistive plasmas is the primary objective of the present work.

In a resistive plasma, the screening effect, or eventually the screening current generated inside the plasma, is a combined result of both the plasma conductivity and the plasma flow. Significant theory and modelling efforts have been devoted to study the plasma response induced screening. Early work is often developed within the cylindrical approximation, and applied mainly to the tearing mode (TM) locking [12, 13, 22], as well as the ELM control related RMP problems [6, 23]. During recent years, significant modelling efforts have been carried out to study the plasma response to the 3D RMP fields in toroidal geometry [24-32].

It is now well established that the detailed screening physics, associated with the plasma flow, depends on the plasma model assumptions. In particular, the single fluid model predicts a strong screening due to the toroidal flow of thermal ions [13, 24], whilst the two fluid theory predicts screening due to the perpendicular (to the magnetic field lines) flow of thermal electrons [26, 27, 33]. In the limit of vanishing speed of the respective flow (at rational surfaces), both models would predict full penetration of the external resonant fields.

However, few modelling work has been performed, in order to understand how the screening changes, as the plasma flow gradually approaches zero near the perturbation rational surface inside the plasma, and how the flow shear affects the results. This is of particular interest following the recent realization that, according to the single fluid theory, at very slow flow, the favorable averaged toroidal curvature effect, which is often associated with the TM stabilization in a toroidal plasma, provides additional screening of the external fields [34]. This work provides the first systematic, numerical investigation of this so called GGJ-screening regime using the MARS-F code [35]. Comparison is also made with the conventional resistive-inertial (RI) regime [13], which occurs at faster flow than the GGJ regime. The results may be relevant for interpreting not only the mode locking experiments, but also the ELM control (in particularly the ELM suppression) experiments using RMP fields at low input toroidal torque.

We shall only consider the single fluid model in this study. The electron flow screening physics may be particularly relevant for studying the RMP penetration problem, where the primary interest is in the H-mode pedestal region. The electron diamagnetic flow is normally large in pedestal. In this work, we are mainly interested in the flow screening for the core TM (at the $q = 2$ surface here), where the electron diamagnetic flow contribution is normally not significant. Even for the typical RMP problem, it seems that the single fluid approximation, including the toroidal flow induced plasma response screening, works satisfactorily well when

compared with experiments [19, 25, 36]. This can be partially explained by the fact that the conventional single fluid flow screening and the perpendicular electron flow screening are essentially equivalent when casted in the proper mathematical formulation, as discussed in Ref. [16].

Section 2 briefly describes the MARS-F single fluid, resistive plasma response model. Section 3 introduces three families of radial profiles for the toroidal rotation frequency of the plasma. Systematic rotation scan study is based on these flow profiles. Section 4 reports the computational results using the first two families of the flow profiles, both assuming unidirectional flow across the whole plasma minor radius. Section 5 reports results with the third family of flow profiles, where we allow the flow reversal near the rational surface. Peculiar screening physics is discovered and studied in this section. Section 6 draws conclusion and discussion.

2. The toroidal, single fluid, resistive plasma response model

We used the MARS-F code [35] to compute the plasma response to the external magnetic field under the dc condition, while prescribing a radial profile for the plasma flow speed $\mathbf{V}_0 = R\Omega\hat{\phi}$, where R is the plasma major radius, Ω is the angular frequency of the toroidal rotation, specified as a function of the plasma minor radius, and $\hat{\phi}$ is the unit vector along the geometric toroidal angle ϕ. MARS-F solves the linearized single fluid, resistive, full MHD equations in a general toroidal geometry.

$$i\left(\Omega_{RMP}+n\Omega\right)\boldsymbol{\xi} = \mathbf{v} + \left(\boldsymbol{\xi}\cdot\nabla\Omega\right)R\hat{\phi} \tag{1}$$

$$i\rho\left(\Omega_{RMP}+n\Omega\right)\mathbf{v} = -\nabla p + \mathbf{j}\times\mathbf{B} + \mathbf{J}\times\mathbf{b} - \rho\left[2\Omega\hat{Z}\times\mathbf{v} + \left(\mathbf{v}\cdot\nabla\Omega\right)R\hat{\phi}\right] \tag{2}$$

$$i\left(\Omega_{RMP}+n\Omega\right)\mathbf{b} = \nabla\times\left(\mathbf{v}\times\mathbf{B} - \eta\mathbf{j}\right) + \left(\mathbf{b}\cdot\nabla\Omega\right)R\hat{\phi} \tag{3}$$

$$i\left(\Omega_{RMP}+n\Omega\right)p=-\mathbf{v}\cdot\nabla P-\Gamma P\nabla\cdot\mathbf{v} \tag{4}$$

$$\mathbf{j}=\nabla\times\mathbf{b} \tag{5}$$

where the variables ξ, $\mathbf{v}$, p, $\mathbf{j}$ and $\mathbf{b}$ denote the plasma displacement, perturbed velocity, pressure, current and magnetic field, respectively. The equilibrium plasma density, magnetic field, pressure and current are denoted by ρ, $\mathbf{B}$, P and $\mathbf{J}$, respectively. n is the toroidal harmonic number. We consider $n=1$ in this study. The equations are written in the dimensionless form, with the length normalized to the major radius of the magnetic axis, the time to the toroidal Alfvén time τ_A, the magnetic field to the on-axis vacuum toroidal field B_0, the pressure to B_0^2/μ_0. The toroidal rotation frequency Ω is normalized to the Alfvén frequency Ω_A.

The external 3D field is generated by the coil currents set in vacuum. In MARS-F code, the coil current density $\mathbf{j}_{RMP}$, as a source term, is prescribed which satisfies Amper's law $\nabla\times\mathbf{b}=\mathbf{j}_{RMP}$. The frequency of the source current is denoted by Ω_{RMP} in Eqs. (1)-(4). This term vanishes if dc coil currents are assumed, as in this study. This is often the case for field errors as well as for the RMP fields in the ELM control experiments.

The above equations are solved in an equilibrium magnetic flux surface based straight field line coordinate system, where the toroidal angle is chosen as the geometric angle. The minor radius is labelled by the equilibrium poloidal flux function. The poloidal angle is chosen such that the jacobian, associated with the transformation from the cylindrical coordinates, is proportional to R^2.

3. Specification of the plasma equilibrium and flow profiles

To facilitate understanding of the numerical results from the MARS-F runs, we shall consider a simple equilibrium, the same as that assumed in Ref. 34. This equilibrium has a single rational surface associated with the $n=1$ perturbation inside the plasma. The radial profile of the equilibrium plasma pressure and the safety factor is shown in figure 1(a) and 1(b), respectively. The radial coordinate is defined as $s \equiv \sqrt{\psi_n}$, with ψ_n being the normalized poloidal flux. Most of the physics effects that we shall study in this work are associated with the $q=2$ rational surface. The GGJ screening effect, occurring at slow flow, is essentially due to the finite equilibrium pressure gradient at the $q=2$ surface.

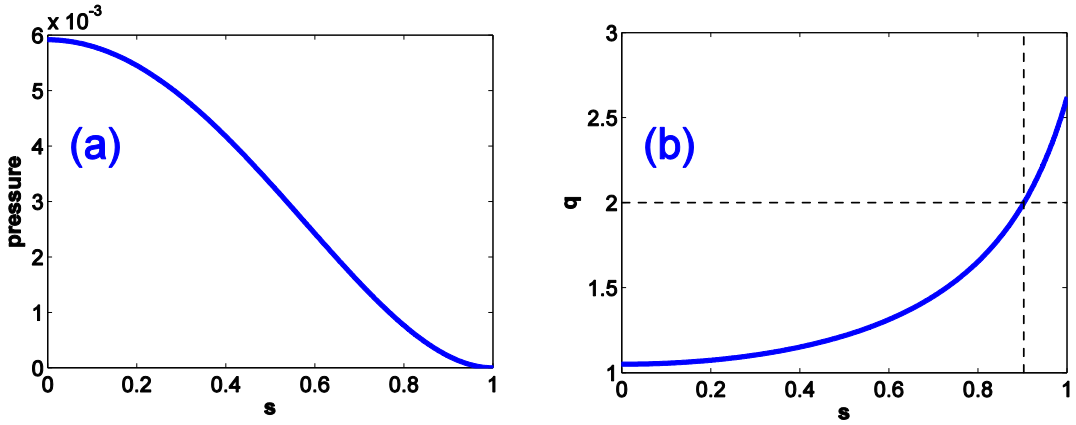

Figure 1. Radial profiles of (a) the plasma equilibrium pressure, and (b) the safety factor. The radial coordinate is the square root of the normalized equilibrium poloidal flux. The vertical dash line in (b) denotes the location of the rational $q=2$ surface.

All results in Ref. 34 were obtained assuming a uniform equilibrium rotation profile. With the primary objective of this work to study the effect of the local flow speed at the rational surface on the plasma screening of the external 3D fields, we wish to understand: (i) what happens if the local flow speed vanishes near or at the perturbation rational surface? (ii) what is the role played by the local flow shear as well as the global flow profile? (iii) what is the difference in the screening as the flow speed approaches zero without or with the reversal of the flow direction?

In order to answer the these questions, we consider various ways of specifying the flow profiles, taking special care of the local variation of the flow profile near the rational surface. More specifically, we choose three families of sheared plasma rotation frequency profiles as shown below.

3.1. Model A: A unidirectional flow with global variation of flow profile

Such a profile is prescribed by the following model

$$\Omega = \left(\Omega_0 - \Omega_1\right)\left(1 - 2s^2 + s^3\right) + \Omega_1 \tag{6}$$

where Ω_0 is the amplitude of the plasma rotation frequency at the magnetic axis, and Ω_1 is defined as the rotation frequency at the plasma surface [24]. An example of such a profile, normalized to unity at the magnetic axis, is shown in figure 2(a). Similar to the magnetic shear, we define the flow shear as

$$S_\Omega = s\left(d\Omega/ds\right)/\Omega$$

Note that if Ω_1 vanishes in Eq. (6), the above defined flow shear is a constant while varying the flow amplitude. In numerical computations, we normally assume a very small edge flow Ω_1. Thus the local flow shear is kept nearly constant, while varying the global flow profile by adjusting the flow amplitude.

3.2. Model B: A unidirectional flow with local variation of flow amplitude

In order to investigate the relative effect of the flow shear and the flow amplitude, at the rational surface, on the plasma response to the external magnetic field, we consider a new family of profiles, with nearly vanishing plasma flow speed at the rational surface. The profile is defined as

$$\Omega = \left| \frac{\Omega_0}{-2s_q^{\,2} + s_q^{\,3}} \left(2s^2 - s^3 - 2s_q^{\,2} + s_q^{\,3} \right) \right| \left[1 - e^{-\left((q-2)/10^{-3}\right)^2} \right] + \Omega_q \qquad (7)$$

where s_q is the radial position of the rational surface $q = 2$, and Ω_q is the plasma rotation frequency at this surface. The model allows a large variation of Ω_q, by orders of magnitude, without significant change of the core rotation Ω_0. In addition, the local flow shear at the rational surface vanishes. Figure 2(b) shows one example of the radial equilibrium plasma rotation frequency profile, where Ω is again normalized to unity at the magnetic axis Ω_0.

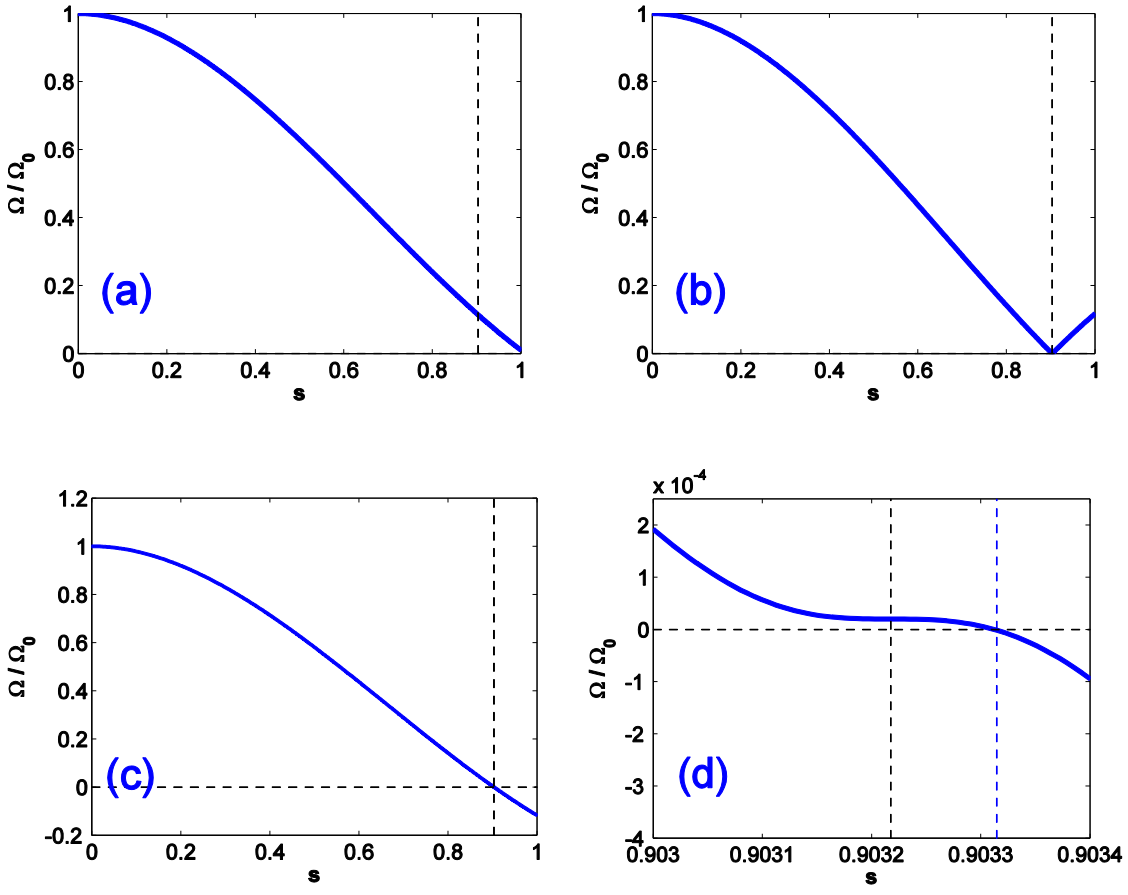

Figure 2. Three types of radial profiles for the equilibrium toroidal rotation frequency of the plasma: (a) without, and (b) with, a strong local variation of the flow profile near the $q = 2$ rational surface, indicated by black dashed vertical lines, (c-d) with reversal of the flow direction, with (d) showing the details near the rational surface. The blue vertical dash line indicates the position of the vanishing flow surface.

Compared to the global flow model as described in subsection 3.1, the above model allows more flexibility in independent variation of the on-axis flow amplitude and the local flow amplitude at the rational surface, at the same time without introducing the flow reversal effect that is described by the next model.

3.3. Model C: A flow profile with local reversal of direction near rational surface

As shall be shown later in this work, the local reversal of the flow direction introduces a subtle degeneracy into the screening physics (the Ohm's law), when the zero-crossing coincides with the radial location of the rational surface. Numerically we investigate the screening in this peculiar situation, by radially separating the zero-crossing surface for the flow and the rational surface. We then gradually decrease the distance between these two surfaces.

The flow model is thus proposed as follows

$$\Omega = \frac{\Omega_0}{-2s_q^{\,2} + s_q^{\,3}}\left(2s^2 - s^3 - 2s_q^{\,2} + s_q^{\,3}\right)\left[1 - e^{-((q-2)/D)^2}\right] + \Omega_q \tag{8}$$

where the definitions of s_q, Ω_q are the same as in Model B. At fixed rotation frequencies on the magnetic axis (Ω_0) and at the rational surface (Ω_q), parameter D controls the distance between the flow reversal surface ($\Omega = 0$) and the rational surface ($q = 2$). Taking $D = 10^{-3}$ for example, Fig. 2(c-d) show the radial rotation profile with definition (8), with figure 2(d) showing the detailed profile near the rational surface. The flow frequency is again normalized to unity on the magnetic axis. In further computations, the on-axis rotation frequency Ω_0 is also one of the scanned parameters.

We note that such a choice of the flow profile (8) again yields vanishing flow shear at the rational surface. Compared to a case without the exponential factor in (8), this choice allows a

larger radial separation between the zero-crossing surface for the flow and the rational surface, while reducing the local flow amplitude at the rational surface. As a result, it becomes easier to isolate the two effects, associated with the distance between the two surfaces on one hand, and the local flow speed at the rational surface on the other hand. The fact that the local flow shear becomes zero is not essential in understanding the screening physics, since as will be shown in the following, the local flow shear does not play a significant role in the screening of the GGJ regime.

Note also that the specification of Model C bears close similarity to that of Model B, allowing comparison between different models. In both Models B and C, the on-axis flow speed Ω_0 and that at the rational surface Ω_q can be independently varied, whilst this is not possible with the flow profile Model A, where the flow speeds on the axis and at the rational surface always change in proportion.

4. Screening due to unidirectional toroidal flow

We have carried out extensive modeling and analysis efforts, in order to identify the screening physics associated with the local variation of the plasma flow speed near the rational surface. The results, computed by the MARS-F code, are summarized in figure 3, showing plasma response amplitude at the $q=2$ surface, for the $m/n=2/1$ resonant harmonic of the perturbed radial field, while scanning the local flow amplitude $\Omega_{q=2}$ at the rational surface. The radial component of the perturbed magnetic field $\mathbf{b}$ is defined as $b^1 = q\left(d\psi/ds\right)\left(\mathbf{b}\cdot\nabla s\right)/\left(\mathbf{B}\cdot\nabla\phi\right)$, where $s=\sqrt{\left(\psi-\psi_{axis}\right)/\left(\psi_{edge}-\psi_{axis}\right)}$. The total field b^1_{tot} produced by both the external coil currents and the perturbed currents of the plasma due to the plasma response. b^1_{vac} is the free-space vacuum field generated by the external coil currents alone, in the absence of the plasma response.

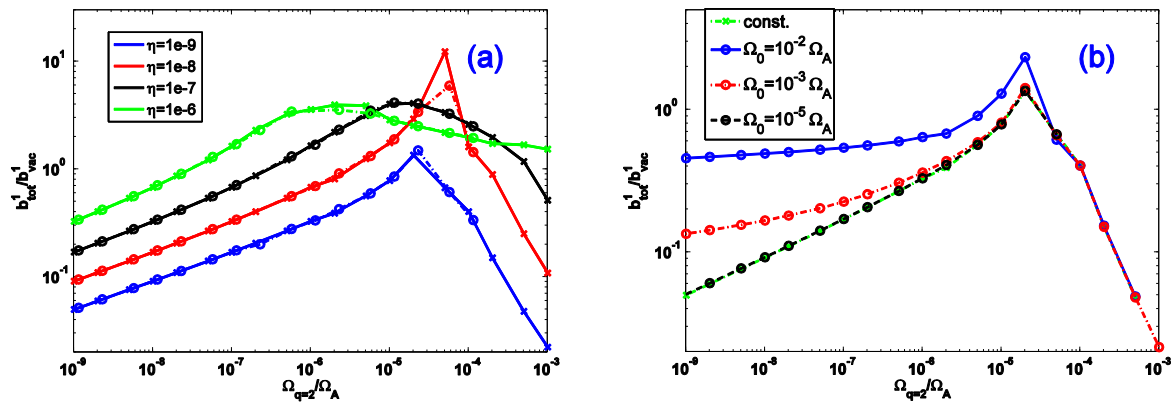

Figure 3. Comparison of the flow screening effects between the uniform flow profile and (a) the flow profile Model A, (b) the flow profile Model B. Plotted is the amplitude of the resonant ($m/n = 2/1$) radial field component including the resistive plasma response, normalized by that of the vacuum field, versus the local flow speed at the $q = 2$ surface. Various values of the normalized plasma resistivity, of constant radial profile, are assumed in (a), where the results with the uniform flow (lines with crosses) are compared with that of Model A flow profile (lines with circles). Various on-axis flow amplitudes, $\Omega_0 = 10^{-2}\Omega_A$, $\Omega_0 = 10^{-3}\Omega_A$ and $\Omega_0 = 10^{-6}\Omega_A$, respectively, are chosen in (b) for the flow profile Model B, at the normalized plasma resistivity $\eta = 10^{-8}$.

Two flow profile models (Model A and B) are used in Fig. 3. Fig. 3(a) compares the plasma response behavior assuming either a uniform flow profile, or the profile Model A at fixed small edge flow speed of $\Omega_1 = 10^{-2}\Omega_0$, with different choices of the plasma resistivity. The resistivity parameter η is defined as a dimensionless number by normalizing the physics quantity to a factor $\mu_0 R_0 v_A / A^2$, with $v_A = B_0 / \sqrt{\mu_0 \rho_0}$, A being the aspect ratio and ρ_0 the on-axis plasma density. Effectively η is the inverse of the Lunquist number. Here a uniform resistivity profile is assumed along the plasma minor radius.

It is interesting to note that, the flow profile model A, which has a finite local flow shear at the rational surface, produces nearly the same screening as that by the uniform flow, indicating that the local flow shear is not important in producing the screening effect. In other words, it is the local flow amplitude that quantitatively determines the resonant field screening. This holds for both screening regimes shown in Fig. 3(a) – the GGJ regime at slow

flow and the RI regime at fast flow. Note that in the GGJ-regime, the response field amplitude decreases (i.e. screening is enhanced) with *decreasing* the plasma flow speed, whilst the opposite occurs in the RI-regime, where the enhanced screening is achieved by *increasing* the flow speed.

The plasma resistivity is another key factor affecting the screening. For both regimes, increasing the plasma resistivity generally reduces the screening.

Model A does not allow strong variation of the local flow profile near the rational surface. A subtle difference appears when such a strong local variation is indeed allowed, as in Model B (Fig. 2(b)). The computed plasma response using this type of flow profile is summarized in Fig. 3(b). Because of the possibility of independently varying the flow speed on the magnetic axis (Ω_0) and at the rational surface ($\Omega_{q=2}$) with Model B, we choose three different values of Ω_0 while scanning $\Omega_{q=2}$. The results are also compared with that of the uniform flow profile. As expected, both the GGJ and the RI screening regimes are again obtained, at slow and fast flow at the rational surface, respectively. An interesting observation is that the separation between these two regimes occurs at the same $\Omega_{q=2}$ value, which is about $2\times10^{-5}\Omega_A$ in our case, independent of the on-axis flow speed Ω_0. This again points to the critical role played by the local flow amplitude, on the plasma response induced screening of the resonant field component.

However, the on-axis flow speed, or in other words the global flow profile, does affect the GGJ screening regime as well. Generally at a fixed rational surface flow, increasing the on-axis flow speed *reduces* the GGJ screening effect. Interestingly, no such effect is seen for the RI screening regime. In order to better understand these two screening regimes, we perform a detailed investigation of the key physics elements that determine the screening.

The flow screening is essentially described by the radial component of the Ohm's law, Eq. (3). It turns out that, with a proper choice of the basis vectors, the radial component of Eq. (3) can be rigorously written for each individual Fourier harmonic (m, n) in a straight field line coordinate system, even for a generic toroidal equilibrium

$$\Omega b^1_{mn} = i\psi'\left(m - nq\right)\Omega\xi^1_{mn} + \eta\left[\frac{JB}{\psi'}\delta J_{\|}\right]_{mn} \tag{9}$$

where b^1_{mn} is the Fourier harmonic of the radial field b^1 as defined before, ξ^1_{mn} is the Fourier harmonic of the radial displacement defined as $\xi^1 = \boldsymbol{\xi}\cdot\nabla s$, $\delta J_{\|}$ is the parallel (to the equilibrium field line) component of the perturbed plasma current, J is the jacobian of the coordinates transformation, B is the equilibrium magnetic field amplitude, and finally $\psi' = d\psi/ds$. In the curve-linear flux coordinate system (s, χ, ϕ), all the perturbed quantities have a $e^{im\chi - in\phi}$ dependence for the (m, n) Fourier harmonics. By representing the perturbed plasma current in the form $\mathbf{j} = j_1\nabla s + j_2\nabla\chi + j_3\nabla\phi$, the parallel component $\delta J_{\|}$ is calculated as

$$\delta J_{\|} = \frac{\psi'}{JB}\left(j_2 + qj_3\right) \tag{10}$$

Representation (9) greatly simplifies the physics analysis of the flow screening effect, without compromising the toroidal coupling effect. Three terms are identified in Eq. (9): the left hand side (*LHS*) term, Ωb^1_{mn}, is related to the radial component of the perturbed magnetic field, indicating the plasma response in terms of the total field; the first right hand side (RHS_1) term, $i\psi'\left(m - nq\right)\Omega\xi^1_{mn}$, is associated with induction, and thus further referred to as the induction term, the second right hand side (RHS_2) term, $\eta\left[JB/\psi'\right]\left[\delta J_{\|}\right]_{mn}$, is the resistive

term in Ohm's law. The eventual amplitude of the plasma response field, i.e. the screening effect, is the combined result of both RHS terms in Ohm's law.

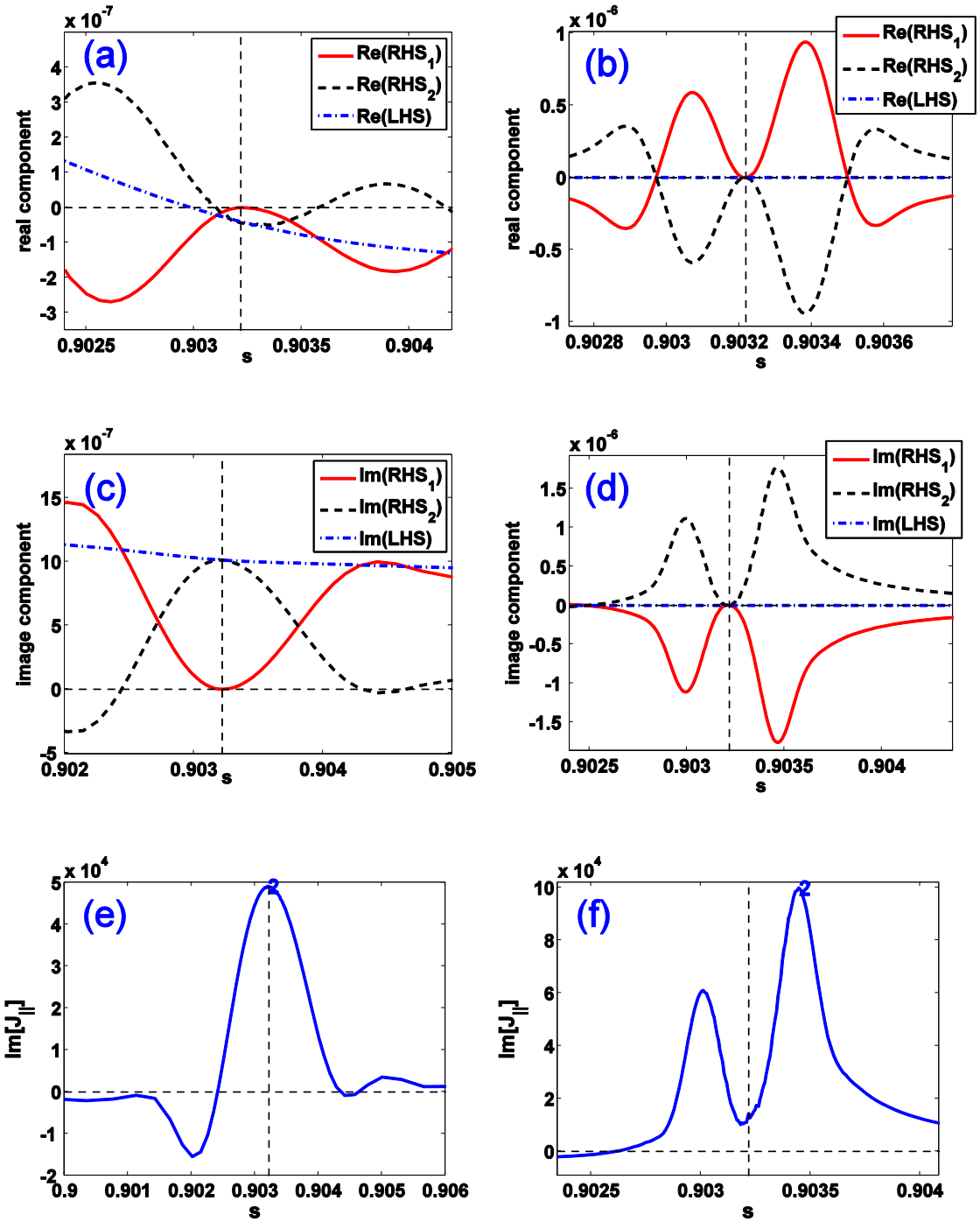

Figure 4. Comparison of key perturbed physics quantities associated with screening, between the RI-regime at fast plasma flow ($\Omega_0 = 10^{-3}\Omega_A$, $\Omega_{q=2} = 10^{-4}\Omega_A$, left panels) and the GGJ-regime at slow flow ($\Omega_0 = 10^{-6}\Omega_A$, $\Omega_{q=2} = 10^{-7}\Omega_A$, right panels). The radial profiles, near the $q = 2$ rational surface indicated by vertical dashed lines, are compared for (a, b) the real, and (c, d) the imaginary, parts of three terms in Eq. (9), representing the

screening contributions from the induction term (RHS_1) and the resistive term (RHS_2) in Ohm's law, and their sum (LHS), and (e, f) the (dominant) imaginary parts of the plasma response generated, $m = 2$ perturbed parallel currents, Eq. (10). The flow profile Model B is assumed, with normalized plasma resistivity of $\eta = 10^{-8}$.

Figure 4 compares all the key physics components, participating into Ohm's law, between the RI regime and the GGJ regime. For two examples based on the flow profile Model A. Similar results are obtained using the flow Model B. The radial distributions of all three terms of Eq. (9), just near the $q = 2$ rational surface, are plotted in Fig. 4(a-d). In the GGJ screening regime (right panels), a large cancellation is observed between the induction term and the resistive term in Ohm's law. It is indeed because of this cancellation, the perturbed radial field is small, resulting in the so called GGJ screening.

On the other hand, no such cancellation occurs in the RI regime (left panels). In this case, the major contribution to the plasma response near the rational surface comes from the resistive term RHS_2.

Since the screening is eventually associated with the plasma generated current perturbation, we also compare the resonant component of the parallel current as defined in Eq. (10). This is shown in Fig. 4(e-f). In the conventional screening regime (figure 4(e)), perturbed parallel current peak is at the rational surface, providing the screening of the externally applied resonant fields. In the GGJ regime (figure 4(f)), however, the perturbed parallel current peaks are off (but very close to) the rational surface. It is eventually these two off-resonant peaks that provide the screening of the external magnetic field in the GGJ regime.

5. Screening due to toroidal flow with local reversal of direction near rational surface

The plasma response is more subtle when the toroidal flow locally switches direction near the rational surface. Numerically we find that a strong singularity occurs in the response solution near the rational surface, as the flow speed crosses zero, switching sign, exactly at the rational

surface. No such singular behavior in the response solution is observed with the flow Model B, as the local flow speed approaches zero exactly at the rational surface.

We attribute the singular solution, associated with the Model C, to the degeneracy of the Ohm's law in Eq. (9). Indeed in the case of Ω approaching zero at the rational surface, the coefficients in the three terms, associated with the perturbed quantities in Eq. (9) (radial field, radial displacement, and parallel plasma current, respectively), approach zero with different orders. This gives constraints on the possible radial distribution near the rational surface, for the perturbed quantities which have to be self-consistently determined (i.e. satisfying all other MHD equations). This can lead to different possibilities for the response solution. The flow Model B based response solution, for instance, resolves the degeneracy in the equilibrium coefficients by the vanishing parallel current perturbation at the rational surface (at finite resistivity η). The self-consistent response solution based on the flow Model C, on the other hand, does not seem to follow the same cancellation rule. As a result, a stronger singularity develops in the solution near the rational surface, which we believe is un-physical, and cannot be numerically resolved.

However, we still have the possibility to study the flow screening in this case, by two means. First, we separate the resonant surface and the surface where the flow vanishes (further referred to as the zero-flow surface), and gradually decrease the radial distance between these two surfaces. Secondly, we consider a resistivity model that also vanishes at the rational surface

$$\eta = \eta_0 \min\left[1, \left(\Omega/\Omega_q\right)^4\right] \tag{11}$$

Such a model, to certain degree, removes the degeneracy of Eq. (9).

Figure 5 summarizes the computed response results, following the aforementioned procedures. Since the radial distance between the rational surface and the zero-flow surface is controlled by the model parameter D in Eq. (8), we show two cases (a) and (b), representing roughly two extreme cases: case (a), with $D = 5\times10^{-3}$, corresponds to the situation where these two surfaces are well decoupled, whilst case (b), with $D = 10^{-3}$, shows the results when the physics effects at these two surfaces start to strongly couple to each other.

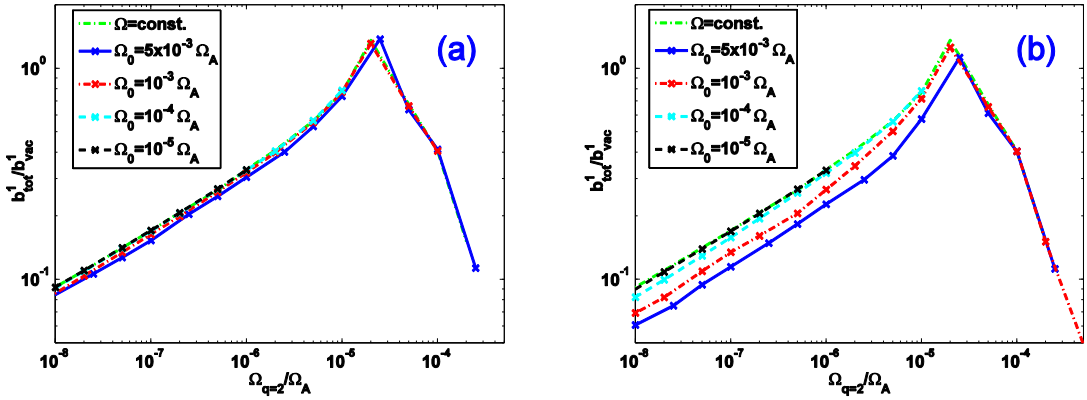

Figure 5. Comparison of the flow screening effects between the uniform flow profile and the flow profile Model C with two choices of the value for the model parameter D: (a) $D = 5\times10^{-3}$, and (b) $D = 10^{-3}$. Plotted is the amplitude of the resonant ($m/n = 2/1$) radial field component including the resistive plasma response, normalized by that of the vacuum field, versus the local flow speed at the *q=2* surface. Different on-axis flow speeds are chosen here in Model C, with $\Omega_0 = 5\times10^{-3}$, $\Omega_0 = 10^{-3}$, $\Omega_0 = 10^{-4}$, $\Omega_0 = 10^{-5}$, respectively. The normalized plasma resistivity is fixed at $\eta = 10^{-8}$.

First, we note that all these subtle physics have almost no effect on the RI screening regime. They do, however, affect the GGJ regime, although the effect is not as significant as that by the flow Model B. Compared to the uniform flow results, the decoupling between the rational surface and the zero-flow surface results in minor modification of the GGJ screening, as shown by Fig. 5(a). On the other hand, the strong coupling effects between the two surfaces do change the GGJ screening as shown in Fig. 5(b). More interestingly, the screening becomes even stronger than the uniform flow case, as the on-axis flow speed is increased.

This is opposite to the results with the flow Model B, where the GGJ screening effect is always weaker than the uniform flow case.

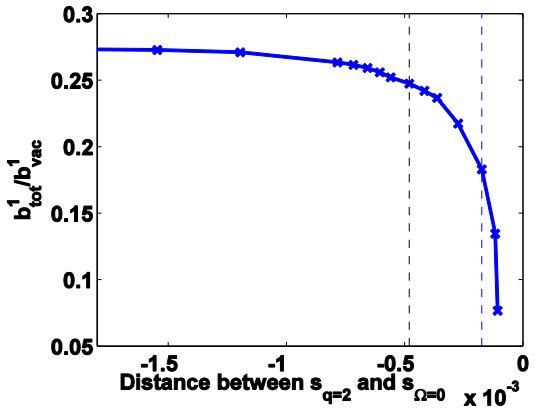

Figure 6. The amplitude of the resonant ($m/n = 2/1$) radial field component including the resistive plasma response, computed assuming the flow profile Model C and normalized by that of the vacuum field, plotted versus the distance between the rational $q = 2$ surface and the vanishing flow surface. This surface is controlled by varying the model parameter D, with the black and blue vertical dashed lines corresponding to $D = 5\times10^{-3}$ and $D = 10^{-3}$, respectively. Fixed are the on-axis flow speed $\Omega_0 = 5\times10^{-3}\Omega_A$, the flow at the rational surface $\Omega_{q=2} = 5\times10^{-7}\Omega_A$, as well as the normalized plasma resistivity $\eta = 10^{-8}$.

In order to demonstrate the sensitive dependence of the flow Model C based GGJ screening, on the separation between the rational surface and the zero-flow surface, Fig. 6 shows the computed resonant response field amplitude versus the radial distance (normalized by the plasma minor radius) between these two surfaces, while scanning the parameter D in Eq. (8) using the flow profile Model C. The response amplitude stays nearly constant as the zero-flow surface is located far away from the rational surface. As the two surfaces radially merge, the plasma response is significantly reduced, resulting in enhanced GGJ screening by the flow reversal near the rational surface.

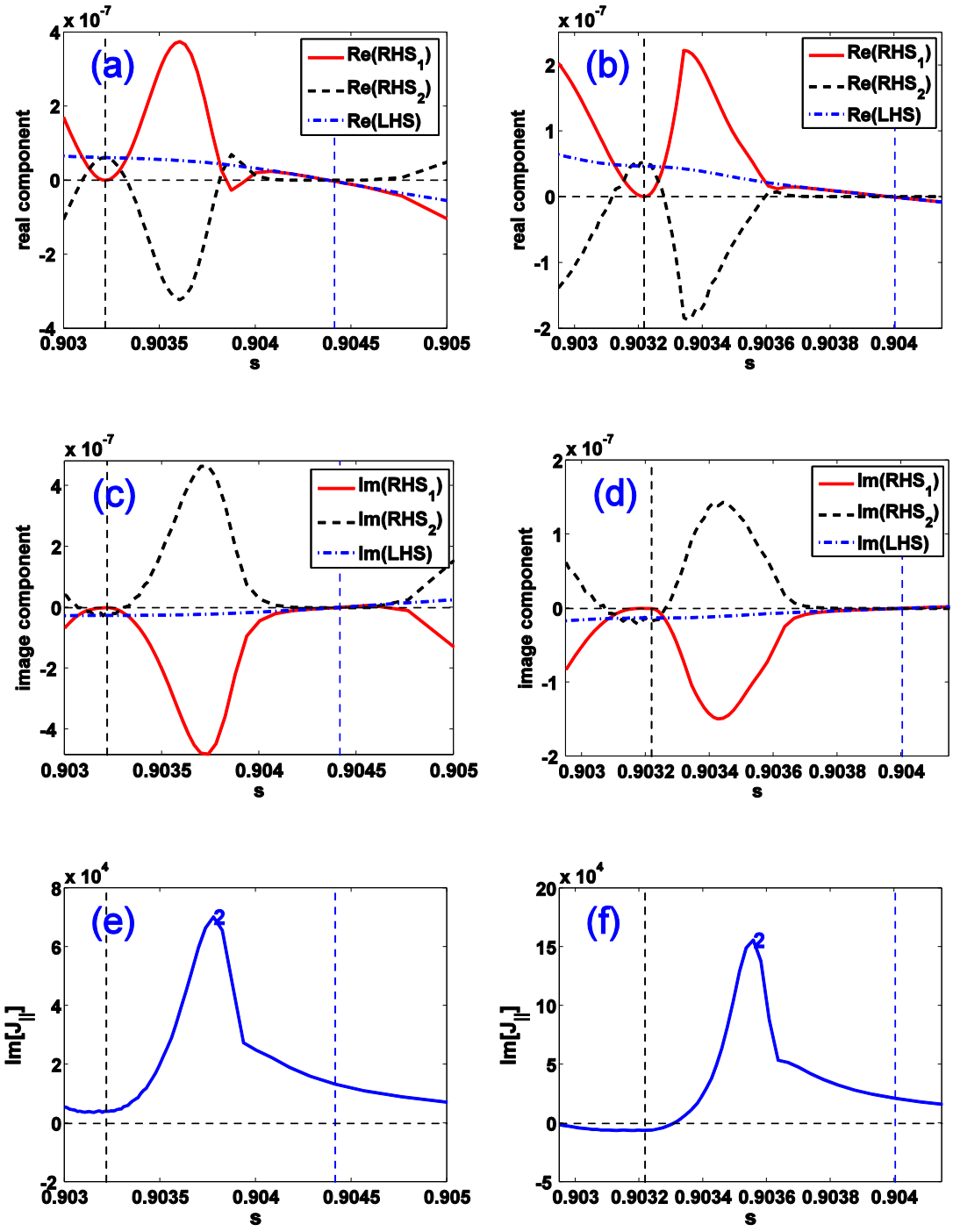

Figure 7. The key perturbed physics quantities associated with screening, computed using the flow profile Model C with two choices of the value for the model parameter D: $D = 5\times10^{-3}$ (left panels) and $D = 10^{-3}$ (right panels). The radial profiles near the $q = 2$ rational surface are compared for (a, b) the real, and (c, d) the imaginary, parts of three terms in Eq. (9), representing the screening contributions from the induction term (RHS_1) and the resistive term (RHS_2) in Ohm's law, and their sum (LHS), and (e, f) the (dominant) imaginary parts of the plasma response generated, $m = 2$ perturbed parallel currents, Eq. (10). The black (blue) vertical dash line indicates the radial location of the rational $q = 2$ (the vanishing flow) surface. Fixed are the on-axis flow speed

$\Omega_0 = 5\times10^{-3}\Omega_A$, the flow speed at the rational surface $\Omega_{q=2} = 5\times10^{-6}\Omega_A$, as well as the normalized plasma resistivity $\eta = 10^{-8}$.

Figure 7 compares the radial distribution of the key quantities participating into the screening physics, assuming the flow profile Model C without (a, c, e) and with (b, d, f) strong coupling effects between the rational surface and the zero-flow surface. The radial distributions of the induction and resistive terms are somewhat similar. There is still a large cancellation between the inductive and the resistive terms in these two cases, both being in the GGJ screening regime. However, the cancellation is less complete than that of the flow profile Model B case. The significant difference between the decoupled surfaces and the coupled surfaces is the amplitude of the plasma generated perturbed parallel current density, shown in Fig. 7(e) and (f), respectively. The coupled case results in about 3 times larger current amplitude, thus stronger screening as shown in Fig. 5 and 6.

6. Conclusion and discussion

This work aim at computational understanding of the plasma induced screening effect on the externally applied 3D resonant magnetic field perturbations, in a situation when the plasma flow becomes small, or even vanishes, at one rational surface of the perturbation. The modelling is carried out using the MARS-F code, which incorporates the single fluid, full MHD, resistive plasma model, with full toroidal geometry. We have considered three families of toroidal flow profiles, representing three typical situations of how the flow speed can approach zero near the rational surface. The key physics here is that the presence of a finite, but very slow flow changes the screening regime within the single fluid MHD theory – from the conventional resistive-inertial type of screening to the so called favorable averaged toroidal curvature induced GGJ screening.

We performed a comprehensive investigation of the subtle and non-trivial screening physics associated with the GGJ effect, in the presence of toroidal flow and flow shear. We find that the local flow amplitude, not the local flow shear, at the rational surface, that is more important in determining the GGJ screening. In addition, the global flow profile also affects the GGJ screening, despite the fact the screening eventually occurs near the rational surface.

An important observation is the nearly perfect cancellation effect between the induction term and the resistive term in Ohm's law, when the GGJ physics is in operation. This is identified as the key physics of the GGJ screening, since the near cancellation between these two terms results in very small amplitude of the resonant radial magnetic field perturbation. On the other hand, such a cancellation does not occur for the RI regime, where the induction term contribution is very small compared to that of the resistive term. These two regimes also significantly differ in terms of the plasma generated screening current. The conventional resistive layer model, which is valid at relatively fast flow, results in a shielding current that peaks at the rational surface, whilst the GGJ model (valid at slow flow) yields a double-peak structure of the perturbed parallel current density along the plasma minor radius. These two peaks occur close but off the rational surface.

We also find that the standard resistive MHD model has an inherent defect in describing the situation where the plasma flow speed vanishes, with the reversal of the flow direction, exactly at the radial location of the perturbation rational surface. Such a degenerated situation leads to un-physical singularity in the plasma response solution. In this study, this degeneracy is resolved by slightly separate the zero-flow surface and the rational surface, and by introducing a peculiar plasma resistivity radial profile, which vanishes at the rational surface, the latter can be viewed as a straightforward, but not unique, way of introducing additional physics into the resistive MHD model without changing the equations. A better model may be obtained by introducing new terms into the equation, such as the hyper-resistivity term in

Ohm's law [37]. We also point out that no such un-physical singularity is numerically found when the flow speed vanishes at the rational surface while keeping unidirectional flow, as described by our second flow profile model.

The GGJ induced screening may offer a possible interpretation of an interesting observation in the mode locking experiments carried out in TEXTOR [38], where the threshold amplitude of the DED current, to induce the mode locking, is experimentally determined while scanning the toroidal flow speed of the plasma in both directions. It was found that a finite minimum DED current threshold is required for the mode locking, even at zero flow speed at the rational surface. The single fluid theory without the GGJ screening always predicts zero DED current thresholds at vanishing flow (corresponding to full penetration). The inclusion of the electron diamagnetic flow cannot offer the explanation either, since this only shifts the location of the minimum DED current, without changing the fact of the existence of the finite current threshold.

The results from this study also predict that, with the right conditions (e.g. the plasma does enter into the GGJ screening regime), a low torque regime (thus slow plasma flow) does not necessarily mean a better ELM suppression regime using the RMP fields. This is because the GGJ screening at slow flow may actually prevent the penetration of the RMP field.

Finally, we emphasize that the single fluid model certainly does not contain all the relevant screening physics, in particular the electron diamagnetic flow and the effects of the (anisotropic) thermal transport terms near rational surfaces [39, 40]. These remain the topics of our future investigation.

Acknowledge

The work was partially supported by the National Natural Science Foundation of China (Grant No. 11405029, 11275047, 11505021). This project has also received funding from the

European Union's Horizon 2020 research and innovation programme under grant agreement number 633053 and from the RCUK Energy Programme [grant number EP/I501045]. The views and opinions expressed herein do not necessarily reflect those of the European Commission.

References

[1] Boozer A H 2001 *Phys. Rev. Lett.* **86** 5059

[2] Liu Y Q 2006 *Plasma Phys. Control. Fu*sion **48** 969

[3] Lanctot M et al 2010 *Phys. Plasmas* **17** 030701

[4] Lanctot M et al 2011 *Phys. Plasmas* **18** 056121

[5] Wang Z R et al 2015 *Phys. Rev. Lett.* **114** 145005

[6] Liu Y Q et al 2000 *Phys. Rev. Lett.* **84** 907

[7] Fransson C M et al 2000 *Phys. Plasmas* **7** 4143

[8] Bondeson A et al 2001 *Nucl. Fusion* **41** 455

[9] Liu Y Q et al 2004 *Nucl. Fusion* **44** 232

[10] Chu M S et al 2010 *Plasma Phys. Control. Fusion* **52** 123001

[11] Liu Y Q et al 2010 *Plasma Phys. Control. Fusion* **52** 104002

[12] Fitzpatrick R et al 1991 *Phys. Fluid B* **3** 644

[13] Fitzpatrick R 1998 *Phys. Plasmas* **5** 3325

[14] Buttery R J et al 1999 *Nucl. Fusion* **39** 1827

[15] Park J-K et al 2011 *Nucl. Fusion* **51** 023003

[16] Liu Y Q et al 2014 *Plasma Phys. Control. Fusion* **56** 104002

[17] Evans T E et al 2006 *Nat. Phys.* **2** 419

[18] Liang Y et al 2007 *Phys. Rev. Lett.* **98** 265004

[19] Kirk A et al 2011 *Plasma Phys. Control. Fusion* **53** 065011

[20] Suttrop W et al 2011 *Phys. Rev. Lett.* **106** 225004

[21] Troyon F et al 1984 *Plasma Phys. Control. Fusion* **26** 209

[22] Yu Q et al 2008 *Nucl. Fusion* **48** 024007

[23] Nardon E et al 2010 *Nucl. Fusion* **50** 034002

[24] Liu Y Q et al 2010 *Phys. Plasmas* **17** 122502

[25] Liu Y Q et al 2011 *Nucl. Fusion* **51** 083002

[26] Bécoulet M et al 2009 *Nucl. Fusion* **49** 085011

[27] Ferraro N M et al 2012 *Phys. Plasmas* **19** 056105

[28] Turnbull A D et al 2013 *Phys. Plasmas* **20** 056114

[29] Haskey S R et al 2014 *Plasma Phys. Control. Fusion* **56** 035005

[30] Haskey S R et al 2015 *Plasma Phys. Control. Fusion* **57** 025015

[31] King J D et al 2015 *Phys. Plasmas* **22** 072501

[32] Ryan D et al 2015 *Plasma Phys. Control. Fusion* **57** 095008

[33] Heyn M F et al 2008 *Nucl. Fusion* **48** 024005

[34] Liu Y Q et al 2012 *Phys. Plasma* **19** 072509

[35] Liu Y Q et al 2000 *Phys. Plasmas* **7** 3681

[36] Kirk A et al 2015 *Nucl. Fusion* **55** 043011

[37] Xu X Q et al 2010 *Phys. Rev. Lett.* **105** 175005

[38] Koslowski H R et al 2006 *Nucl. Fusion* **46** L1

[39] Lutjens H et al 2001 *Phys. Plasma* **8** 4267

[40] Connor J W et al 2015 *Plasma Phys. Control. Fusion* **57** 065001